# Energetics and optical properties of nitrogen impurities in $SrTiO_3$ from hybrid density-functional calculations

Pakpoom Reunchan,[1,*] Naoto Umezawa,[2] Anderson Janotti,[3] Jiraroj T-Thienprasert,[1] and Sukit Limpijumnong[4,†]

[1]*Department of Physics, Faculty of Science, Kasetsart University, Bangkok 10900, Thailand*

[2]*International Center for Materials Nanoarchitectonics, National Institute for Materials Science (NIMS), 1-1 Namiki, Tsukuba, Ibaraki 305-0044, Japan*

[3]*Department of Materials Science and Engineering, University of Delaware, Newark, Delaware 19716, USA*

[4]*School of Physics, and NANOTEC-SUT Center of Excellence on Advanced Functional Nanomaterials, Suranaree University of Technology, Nakhon Ratchasima 30000, Thailand*

(Received 5 December 2016; revised manuscript received 17 March 2017; published 30 May 2017)

Semiconductor photocatalysts that can produce hydrogen from water splitting are of great interest. Among the various possibilities, nitrogen (N)-doped $SrTiO_3$ is a promising candidate for hydrogen evolution under visible-light irradiation. In this study, hybrid density-functional calculations are employed to investigate the stability and impact of nitrogen impurities on the electronic and optical properties in $SrTiO_3$. We find that the substitutional N on O site ($N_O$) is a deep acceptor in $SrTiO_3$. Moreover, $N_O$ predominates over other N-related defects under equilibrium growth conditions in *n*-type $SrTiO_3$. Our results reveal that $N_O$ gives rise to visible-light absorption in agreement with experimental observations. In addition, we find that hydrogen can bind to $N_O$, forming $N_O$-$H_i$ complex which leads to a blueshift in the optical absorption. Other N configurations can also contribute to optical absorption in the visible range. The vibration frequencies of different N configurations are provided to support identification using vibrational spectroscopy techniques.

DOI: 10.1103/PhysRevB.95.205204

## I. INTRODUCTION

The discovery of photocatalytic water splitting on the $TiO_2$ surface [1] has triggered numerous studies on various oxide semiconductors for applications ranging from pollutant degradation to fuel production [2]. Photocatalysis starts with the creation of an electron-hole pair by exciting an electron from the valence band to the conduction band through photon absorption. Therefore, the band gaps of these oxides must be sufficiently wide so that their band-edge positions straddle the reduction and oxidation potentials of the desired chemical compounds.

Recently, $SrTiO_3$ has been suggested as an alternative material to $TiO_2$ for photocatalytic water splitting because of its electronic structure and high chemical stability compared to $TiO_2$. The conduction band edge of $SrTiO_3$ is 0.8 eV higher than the standard hydrogen electrode potential [3], resulting in a stronger reduction potential than that of $TiO_2$. This allows higher efficiency for $H_2$ production and the possibility for overall water splitting without external bias voltage. Nevertheless, only a small fraction of the solar spectrum, i.e., the near-ultraviolet region, is absorbed because of the wide band gap of $SrTiO_3$, which hinders its full photocatalytic efficiency.

This drawback has triggered efforts to tailor the electronic structure of $SrTiO_3$ in order to enhance visible-light absorption. Doping and alloying are widely adopted methods for narrowing the absorption edge of semiconductors. In fact, $SrTiO_3$ doped with noble metals [4] and chromium (Cr) [5–8] has been reported to increase visible-light absorption while retaining the photocatalytic capability. However, these metal dopants often induce trapping levels in the band gap that act as recombination centers and reduce a significant amount of photoexcited carriers. In contrast, nonmetal doping was proposed as an alternative strategy to improve visible-light absorption while retaining the desired photocatalytic ability. This is because they are not expected to induce trapping levels in the band gap. In fact, the incorporation of N impurities has been shown to enhance visible-light absorption [9,10] and improve the photocatalytic activity [11–18].

Despite the intense experimental work focusing on the visible-light absorption and photocatalytic properties of N-doped $SrTiO_3$, the behavior of the N impurities and the actual mechanism underlying visible-light absorption remains ambiguous. Attempts to understand the cause of visible-light absorption have been reported through density-functional calculations. The predominant configuration of the N dopant is generally assumed to be N substituting for O ($N_O$), which introduces occupied states above the valence band that lead to visible-light transitions [9,15,19]. Alternative models, such as cation-N codoping [20–24] and anion-N codoping [24–26], have also been proposed to improve visible-light absorption for specific applications. These models have been further used in the development of visible-light-response $SrTiO_3$-based photocatalysts.

However, analysis of the reported calculations has been primarily based on single-particle energies, i.e., electronic band structure and density of states. Moreover, the N impurities were considered only in their neutral charge state. In fact, the energetics of the N impurities under different growth conditions, as well as their optical properties, have not been well understood. The x-ray photoemission spectra of N 1*s* peaks were assigned to confirm the presence of N–Ti, N–O, and N–N bonds in N-doped $SrTiO_3$ [9,17,27], implying that

*pakpoom.r@ku.ac.th
†sukit@sut.ac.th

 

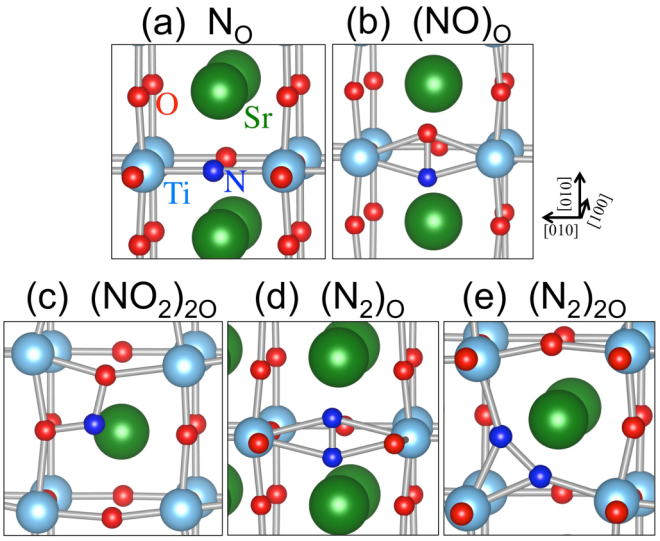


FIG. 1. Local atomic structures of N impurities in $SrTiO_3$: (a) $N_O$, (b) $(NO)_O$, (c) $(NO_2)_{2O}$, (d) $(N_2)_O$, and (e) $(N_2)_{2O}$.

there are at least three configurations of N impurities in the samples. However, the predominant configurations for the N impurities and their effects on electrical and optical properties are still unclear. A stability analysis based on chemical potentials, reflecting the growth conditions, transition levels, and configuration coordinate diagrams derived from the formation-energy difference, has been shown to be an effective tool for investigating the energetics and optical properties of dopant-related defects [28,29]. Although $N_O$ in anatase and rutile $TiO_2$ has been recently revealed as a deep acceptor that results in an impurity-to-band transition in the visible region, consistent with experimental observations [28], the behavior and role of N impurities in $SrTiO_3$ remain controversial.

In the present article, we investigate the energetics as well as the electrical and optical properties of plausible N configurations in $SrTiO_3$, including $N_O$, $(NO)_O$ split-interstitial, $(NO_2)_{2O}$, $(N_2)_O$ split-interstitial, and $(N_2)_{2O}$ complex defects (Fig. 1) through hybrid density-functional calculations. The optical and thermodynamic transitions are determined based on the calculations of the formation energies and configuration coordinate diagrams. We find that N prefers to occupy the O site ($N_O$) in *n*-type $SrTiO_3$, where the Fermi level position is near the conduction band, under O-poor, intermediate, and O-rich conditions. The localized states induced by $N_O$ above the valence band give rise to the optical transition $N_O^- + h\nu \rightarrow N_O^0 + e^-$, which explains the visible-light absorption observed in the experiments. In addition, we consider the effects of hydrogen impurity, which is ubiquitous and could be unintentionally incorporated during growth or processing, by examining the interactions between the H and N impurities. Our calculations show that H binds to $N_O$, forming a $N_O$-$H_i$ complex. In $SrTiO_3$, this complex only results in a relatively small blueshift of the optical absorption, unlike in the case of $TiO_2$, where this type of complex eliminates the effects of $N_O$ on the visible-light absorption [28]. Moreover, $(NO_2)_{2O}$, $(N_2)_O$ split-interstitial, and $(N_2)_{2O}$ defect complexes are also predicted to absorb light in the visible range. Finally, we calculated the vibrational frequencies of N-related defects to aid in the experimental identification of these defects.

## II. COMPUTATIONAL METHOD

Our density-functional calculations were based on the Heyd-Scuseria-Ernzerhof (HSE) [30] hybrid functional, as implemented in the VASP code [31]. In this study, Sr $4s^2 4p^6 5s^2$, Ti $3d^3 4s^1$, O $2s^2 2p^4$ and the N $2s^2 2p^3$ were treated as valence electrons within the projector-augmented wave method [32]. The use of the Hartree-Fock mixing parameter of 28% in the HSE approach yielded an indirect band gap ($R$-$\Gamma$) of 3.27 eV, in good agreement with the experimental value of 3.25 eV [33]. The calculated lattice parameter of 3.913 Å was very close to the experimental value of 3.905 Å for cubic $SrTiO_3$ [34]. The HSE functional has been widely adopted in studies of defects and impurities in wide-band-gap semiconductors with overall excellent agreement between theory and experiment [28,35]. For the studies of N impurities, we employed a 90-atom supercell, which is a $3\times3\times2$ repetition of the 5-atom primitive cell of cubic $SrTiO_3$, with a $2\times2\times2$ mesh of special $k$ points. The energy cutoff for the plane-wave basis-set expansion was set to 400 eV. To ensure the supercell size convergence, test calculations using 135- and 160-atom supercells have been performed for the case of $N_O$. The results are consistent with that obtained from a 90-atom supercell. In addition, test calculations for $SrTiO_3$ in the tetragonal structure (antiferrodistortive phase; space group $I4/mcm$) indicated that the structural instability associated with the $TiO_6$ octahedra rotation under low temperatures does not significantly affect the formation energies of N defects and our main conclusion.

The likelihood of forming substitutional, interstitial, or other configurations of the N impurity was determined by the formation energy as a function of the oxygen ($\mu_O$) and nitrogen ($\mu_N$) chemical potentials for all possible charge states. We calculated the thermodynamic transition level and optical transitions following the standard procedure described in Ref. [36]. For example, the formation energy of $N_O$ in charge state $q$ is given by

$$E^f\left(N_O^q\right) = E_{\rm tot}\left(N_O^q\right) - E_{\rm tot}(SrTiO_3) - \mu_N + \mu_O + qE_F + \Delta^q, \quad (1)$$

where $E_{\rm tot}(N_O^q)$ is the total energy of the supercell containing one N substituted for an O($N_O$), and $E_{\rm tot}(SrTiO_3)$ is the total energy of the perfect crystal using the same supercell. The O atom that is removed from the supercell is placed in a reservoir with energy $\mu_O$, which is referenced as the total energy per atom of an isolated $O_2$ molecule ($\mu_O = \tilde{\mu}_O + \frac{1}{2}E_{\rm tot}[O_2]$), and the N atom is taken from a reservoir with energy $\mu_N$, which is referenced as the total energy per atom of an isolated $N_2$ molecule ($\mu_N = \tilde{\mu}_N + \frac{1}{2}E_{\rm tot}[N_2]$). The chemical potentials $\tilde{\mu}_X$(X = Sr,Ti,O,N,H) are treated as variables and can be appropriately chosen to represent the experimental conditions during growth or annealing. The Fermi level $E_F$ is the electron chemical potential, which is referenced as the valence band maximum (VBM). We applied a charge-state-dependent correction ($\Delta^q$) due to the finite size of the supercell following

the approach in Ref. [37]. However, $\Delta^q$ is very small due to the large static dielectric constant of $SrTiO_3$. The formation energies of the other N configurations and N-H complexes in various charge states are obtained using the same approach.

The chemical potentials $\tilde{\mu}_{Sr}$, $\tilde{\mu}_{Ti}$, and $\tilde{\mu}_O$ must satisfy the stability condition of $\tilde{\mu}_{Sr} + \tilde{\mu}_{Ti} + 3\tilde{\mu}_O = \Delta H_f(SrTiO_3)$, where $\Delta H_f(SrTiO_3)$ is the enthalpy of formation of $SrTiO_3$ with the calculated value of $-16.2$ eV. Their values were taken with respect to the total energy per atom of metallic Sr (fcc), metallic Ti (hcp), and $O_2$ molecule. Bounds were imposed to $\tilde{\mu}_{Sr}$, $\tilde{\mu}_{Ti}$, and $\tilde{\mu}_O$ in order to avoid the formation of secondary phases. For example, the formation of SrO was prevented by including the constraint $\tilde{\mu}_{Sr} + \tilde{\mu}_O < \Delta H_f(SrO)$. Similar constraints were applied to the formation of other relevant limiting phases, i.e., $SrO_2$, $TiO_2$, TiO, and $Ti_2O_3$ [29].

In this article, we present results of the formation energies for O-rich, intermediate, and O-poor conditions. The O-rich and O-poor conditions corresponded to the oxygen chemical potential of $\tilde{\mu}_O = 0$ and $\tilde{\mu}_O = [\Delta H_f(SrTiO_3) - \tilde{\mu}_{Ti} - \tilde{\mu}_{Sr}]/3 = -5.27$ eV, respectively. For the intermediate condition, the O chemical potential is chosen to reflect the growth conditions in Ref. [16]. Based on the growth temperature of 1100 °C and the pressure of 1 atm, we found $\tilde{\mu}_O = -1.57$ eV [8]. Under O-rich and intermediate (experimental) growth conditions, $\tilde{\mu}_N$ is limited by the formation of the $N_2$ molecule, i.e., $\tilde{\mu}_N = 0$, while under the O-poor (Ti-rich) growth condition, $\tilde{\mu}_N$ is limited by the formation of solid TiN, i.e., $\tilde{\mu}_N = \Delta H_f(TiN) - \tilde{\mu}_{Ti}$. Note that the formation of NO, $N_2O$, and $NO_2$ molecules is not relevant in determining $\tilde{\mu}_N$ under any considered growth condition. Under O-rich and experimental conditions, the solubility of H-related defects is limited by the formation of $H_2O$, i.e., $\tilde{\mu}_H = [\Delta H_f(H_2O) - \tilde{\mu}_O]/2$, while under O-poor conditions (metal-rich), the solubility is limited by the formation of solid $SrH_2$, i.e., $\tilde{\mu}_H = [\Delta H_f(SrH_2) - \tilde{\mu}_{Sr}]/2$.

## III. RESULTS AND DISCUSSION

### A. Substitutional N at O site ($N_O$)

The calculated formation energies for $N_O$, $(NO)_O$, $(NO_2)_{2O}$, $(N_2)_O$, and $(N_2)_{2O}$ for the O-poor, intermediate (experimental), and O-rich conditions are shown in Fig. 2. The formation energies for other conditions could be constructed, if needed, using the set of O and N chemical potentials. Our calculated formation energies indicated that $N_O$ is the prevalent defect for Fermi-level values near the conduction band for all considered conditions. $N_O$ is expected to be an acceptor in $SrTiO_3$ because N has one fewer valence electron than O, and $N_O$ can be stable in either the neutral or negative charge states. As shown in Fig. 2, $N_O$ is stable in neutral ($N_O^0$) and negative charge states ($N_O^-$), where the negative charge state is the most energetically favorable defect for Fermi-level values near the conduction-band minimum. This conclusion remains valid for all possible values of O chemical potentials between O-rich and O-poor values. The thermodynamic transition level $(0/-)$ is located at 1.51 eV above the VBM, indicating that $N_O$ is a deep acceptor. This result is similar to the behavior of $N_O$ in ZnO [38] and $TiO_2$ [28], indicating that $N_O$ cannot give $p$-type conductivity in $SrTiO_3$.

The optical properties of the $N_O$ center were determined through the configuration coordinate diagram, as shown in Fig. 3(a). The optical transitions associated with $N_O$ occur through the process $N_O^- + h\nu \rightarrow N_O^0 + e^-$, in which $N_O^-$ absorbs a photon, converting it to $N_O^0$ with an electron in the conduction band. The absorption energy was obtained by calculating the difference in the formation energy between $N_O^0$ in the $N_O^-$ lattice geometry and $N_O^-$ for $E_F$ at the conduction band, and the calculated absorption energy corresponds to the $N_O$-related absorption peak. We found that $N_O$ led to a sub-band-gap optical absorption peak centered at 2.46 eV, in which an electron is excited from the fully occupied states

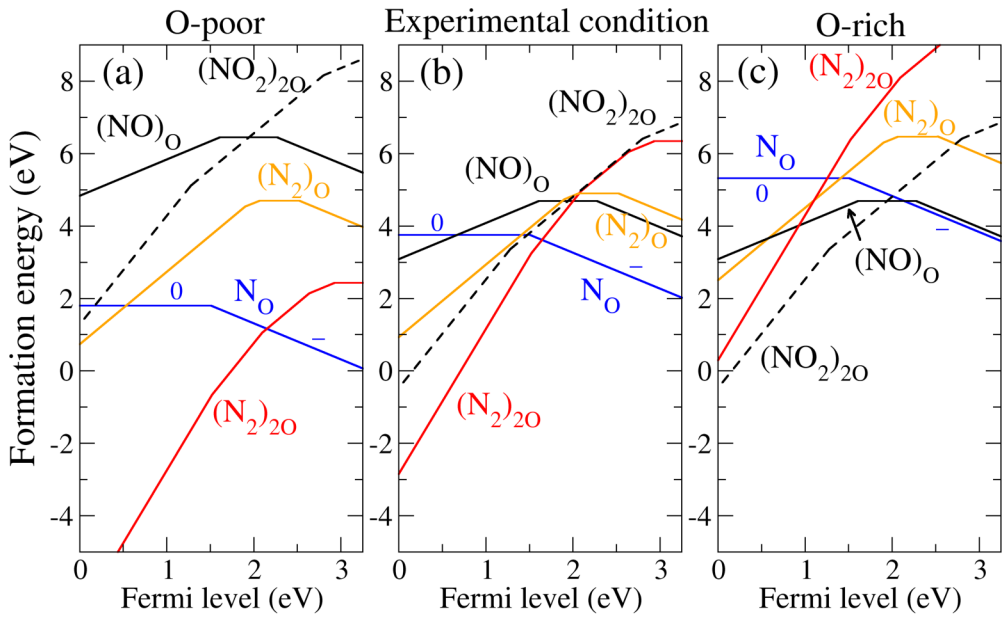


FIG. 2. Formation energies of N-related defects as a function of the Fermi level ranging from 0 to the calculated band gap of 3.27 eV under (a) O-poor, (b) experimental, and (c) O-rich growth conditions. The slopes of the line indicate the charge states of the defects.

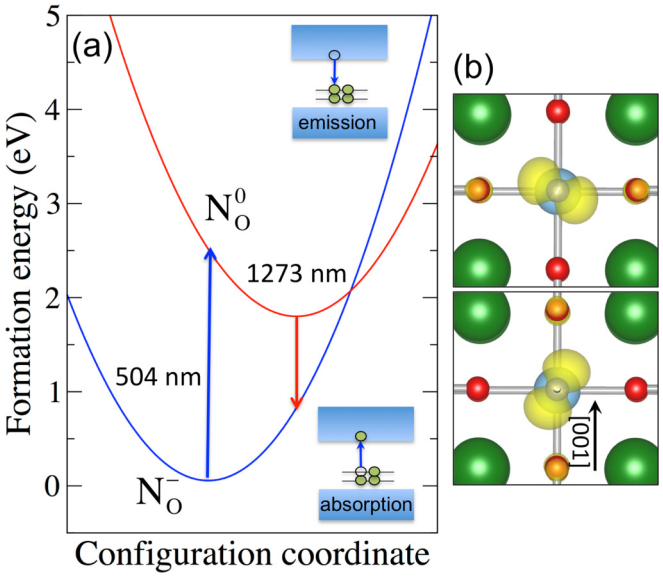


FIG. 3. (a) Configuration coordinate diagram for $N_O$. The formation energies correspond to the similar O-poor condition in Fig. 2(a) and to $E_F$ at the conduction-band minimum. (b) Charge distribution of $N_O$ $2p$ states associated with the optical transition.

of $N_O^-$ [Fig. 3(b)] to the conduction band. Our calculated absorption energy of 2.46 eV is in good agreement with experimental observations in which the absorption edge was reported at about 500 nm (∼2.48 eV) [9,10]. The calculated emission energy, representing the recombination of an electron in the conduction band with the hole in $N_O^0$, i.e., $N_O^0 + e^- \rightarrow N_O^- + h\nu$, is 0.97 eV. This large difference between the absorption and emission energy reflects a large Stokes shift, originating from a large local atomic relaxation associated with $N_O^0$ and $N_O^-$. We found that the Ti atoms surrounding $N_O^0$ relax outward by 1.53% with respect to the equilibrium Ti–O bond length, while the Ti atoms surrounding $N_O^-$ relax inward by 4.20%. This large difference in the local atomic relaxations also indicated that the absorption and emission peaks are expected to be broad. We also considered the transition through the process $N_O^0 + h\nu \rightarrow N_O^- + h^+$ in which an electron is transferred to $N_O^0$, converting it into $N_O^-$ with a hole in the valence band. The absorption energy was calculated by constructing the configuration coordinate diagram in the same way as that shown in Fig. 3(a), yielding a value of 2.28 eV, which was slightly less than the absorption energy associated with the conduction band electron exchange. This value is in good agreement with a recent experimental optical band gap of 2.31 eV measured on N-bombarded $SrTiO_3$ [17]. In these experiments, the Fermi level is likely pinned near the $(0/-)$ transition level of $N_O$, leading to a non-negligible concentrations of $N_O^0$. Both processes lead to visible-light absorption, albeit the process centered on $N_O^-$ yields a slightly higher absorption energy than the process centered on $N_O^0$. In $n$-type $SrTiO_3$, however, the process involving excitation of $N_O^-$ is dominated and likely to contribute to photocatalytic processes in which an electron is excited to the conduction band.

### B. Nitrogen interstitial

We found that interstitial $N(N_i)$ is energetically stable in the form of the $(NO)_O$ split interstitial [Fig. 1(b)] in which N forms a bond with a host O atom by sharing its site. This configuration has been reported to be favorable for N interstitials in other wide-band-gap oxides. Moreover, $(NO)_O$ introduced partially occupied levels in the band gap from which an electron could be either removed or added. Figure 2 shows that $(NO)_O$ occurs in 1+, neutral, and 1− charge states with $(+/0)$ and $(-/0)$ transition levels located at 1.61 and 2.28 eV, respectively. Under O-poor conditions, $(NO)_O$ has a much higher formation energy than $N_O$ for all values of Fermi levels. Under O-rich conditions, $(NO)_O$ has only a slightly higher formation energy than $N_O$ in $n$-type material. Therefore, $(NO)_O$ should not form in a significant concentration because of its relatively high formation energy. When formed, the optical transition can take place via the processes $(NO)_O^- + h\nu \rightarrow (NO)_O^0 + e^-$, in which an electron from $(NO)_O^-$ is excited to the conduction band, and $(NO)_O^0 + h\nu \rightarrow (NO)_O^- + h^+$, in which an electron is excited from the valence band to $(NO)_O^0$. The calculated absorption energies for these two processes are 2.05 and 3.07 eV, respectively. Interstitial N in the form of $(NO)_O$ is not likely to be responsible for visible-light absorption due to its high formation energy.

In addition to the split-interstitial configuration, we found that N can bind with two nearby host O atoms, forming a $NO_2$-like configuration $(NO_2)_{2O}$ [Fig. 1(c)], which is energetically stable in the 1+, 2+, and 3+ charge states. Under O-rich conditions, $(NO_2)_{2O}$ has a relatively low formation energy for Fermi-level positions below ∼1.9 eV with respect to the VBM [Fig. 2(c)], indicating that it could exist with a significant amount in $SrTiO_3$ grown under high oxygen partial pressures. Optical transitions of $(NO_2)_{2O}$ can take place via the processes $(NO_2)_{2O}^{2+} + h\nu \rightarrow (NO_2)_{2O}^{3+} + e^-$, in which an electron is excited from $(NO_2)_{2O}^{2+}$ to the conduction band, and $(NO_2)_{2O}^{3+} + h\nu \rightarrow (NO_2)_{2O}^{2+} + h^+$, in which an electron is excited from the valence band to $(NO_2)_{2O}^{3+}$. These processes yield the absorption energies of 2.80 and 2.19 eV, respectively. $(NO_2)_{2O}$ can possibly contribute to optical absorption in the visible-light region in some $SrTiO_3$ samples.

### C. $(N_2)_O$ split interstitial

An extra N can bind with $N_O$, forming a $(N_2)_O$ split interstitial as shown in Fig. 1(d). We found that $(N_2)_O$ is stable in 2 + ,1+, neutral, and 1− charge states with transition levels $(+2/+)$,$(+/0)$ and $(0/-)$ located 1.90, 2.07, and 2.52 eV above the VBM, respectively. The optical absorption associated with $(N_2)_O$ can take place through the process $(N_2)_O^{2+} + h\nu \rightarrow (N_2)_O^+ + h^+$, in which an electron in the valence band is excited into $(N_2)_O^{2+}$, converting to $(N_2)_O^+$ and a hole. The calculated absorption energy is 2.74 eV, which is larger than the absorption energy associated with $N_O$. The emission energy associated with the recombination of electron from $(N_2)_O^+$ and hole in the valence band is 1.23 eV. Figure 2 shows that $(N_2)_O$ is not the lowest energy configuration for all Fermi-level positions under the considered growth conditions and thus may not occur in high concentration. Even under high-N doping conditions, i.e., N chemical potential higher

than zero, $(N_2)_O$ is not a dominant defect. The formation energies for $(N_2)_O$ and other N-related defects for a high nitrogen chemical potential are shown in Fig. S1 in the Supplemental Material [39]. Based on the calculated formation energy, $(N_2)_O$ is not likely to be responsible for visible-light absorption in N-doped $SrTiO_3$ samples.

### D. $(N_2)_{2O}$ complex

We also investigated the interaction between the two nearby substitutional N on O sites ($N_O$-$N_O$). We found that, through large lattice relaxations, the two $N_O$ are coupled and spontaneously combined into a $N_2$ dimer configuration. This complex is denoted as $(N_2)_{2O}$ and shown in Fig. 1(e). Recently, the coupling of two $N_O$ in $TiO_2$ [40] and $SrTiO_3$ [26] has been studied; however, the energetics of $(N_2)_{2O}$ were not studied in charge states other than neutral or under different growth conditions, and the optical absorption was determined based on calculating the absorption coefficient using dielectric tensors. In the neutral charge state, $(N_2)_{2O}$ introduces two fully occupied states in the band gap. These electrons can be removed when the Fermi level moves toward the valence band. Thus, $(N_2)_{2O}$ can be stable in $4+, 3+, 2+, 1+$, and neutral charge states with the transition levels $(4+/3+), (3+/2+), (2+/+)$, and $(+/0)$ at 1.52, 2.09, 2.64, and 2.93 eV above the VBM, respectively. Because the substitution of two O atoms is involved in the creation of $(N_2)_{2O}$, under O-poor conditions, $(N_2)_{2O}$ has a lower formation energy than $(N_2)_O$ for all possible Fermi-level positions. In addition, we examined the relative stability of the $(N_2)_{2O}$ complex with respect to two isolated $N_O$ by calculating the binding energy defined as $E_b = 2E^f[N_O^0] - E^f[(N_2)_{2O}^0]$. A positive binding energy means that the neutral $(N_2)_{2O}$ is lower in energy than the isolated neutral $N_O$. Our calculated binding energy for $(N_2)_{2O}$ in $SrTiO_3$ was 1.17 eV, which is slightly smaller than the value reported in Ref. [26]. To examine the optical transitions associated with $(N_2)_{2O}$, we considered processes involving an electron transfer from the valence band to the defect state and from the defect state to the conduction band, i.e., (1) $(N_2)_{2O}^{3+} + h\nu \rightarrow (N_2)_{2O}^{2+} + h^+$, in which an electron is excited from the valence band into $(N_2)_{2O}^{3+}$, leaving a hole in the valence band; (2) $(N_2)_{2O}^{3+} + h\nu \rightarrow (N_2)_{2O}^{4+} + e^-$, in which an electron is excited from $(N_2)_{2O}^{3+}$ to the conduction band; (3) $(N_2)_{2O}^{4+} + h\nu \rightarrow (N_2)_{2O}^{3+} + h^+$, in which an electron is excited from the valence band into $(N_2)_{2O}^{4+}$, leaving a hole. Processes (1), (2), and (3) yield the absorption energies of 2.77, 2.61, and 2.52 eV, respectively, all of which are in the visible-light region. Figure 2 shows that $(N_2)_{2O}$ and $N_O$ are dominant defects under O-poor and experimental conditions. At a Fermi level, at which the two formation energy lines for $N_O$ and $(N_2)_{2O}$ intersect, the concentrations of $(N_2)_{2O}$ and $N_O$ are nearly identical. In other words, $N_O$ and $(N_2)_{2O}$ can comparably contribute to the light absorption in the visible range in $SrTiO_3$ samples with Fermi-level positions at 2.15 and 1.63 eV for O-poor and experimental conditions, respectively. Note that the formation energy of $(N_2)_{2O}$ decreases twice as quickly as that of $N_O$ when the N chemical potential is increased. Therefore, in the case of high-N doping, $(N_2)_{2O}$ can become the dominant defect over a wider range of Fermi levels (see Fig. S1) [39]. We thus cannot exclude $(N_2)_{2O}$ as a source of visible-light absorption in N-doped $SrTiO_3$.

Figure 2 shows that $(N_2)_{2O}$, which is a quadruple donor, can be a compensating center for a $N_O$ acceptor under O-poor and experimental conditions. Under these conditions, the Fermi level is pinned near the intersections of the two formation energy lines for the predominant N-related defects, $N_O$ (acceptor) and $(N_2)_{2O}$ (donor), at which a charge neutrality of the system is nearly satisfied among negatively charged $N_O$ and positively ionized $(N_2)_{2O}$. Note that intrinsic free electron and hole carriers can be safely neglected in determining the pinned Fermi level because of the wide band gap of $SrTiO_3$. These pinned Fermi levels, located in the middle of the band gap far away from the VBM, indicate that the hole concentration is extremely low. Combining our results for $N_O$, which is a deep acceptor, and $(N_2)_{2O}$, which acts as active compensating center, we believe that N-doped $SrTiO_3$ cannot be $p$ type under these conditions.

### E. Hydrogen-$N_O$ interaction

Because hydrogen is a ubiquitous impurity and has been reported to play an important role in the electrical properties of many oxides, it is worthwhile to consider the interactions between hydrogen and N in $SrTiO_3$. First, we found that interstitial H ($H_i$) prefers to bind with a host O without introducing any state in the band gap. Interstitial H is exclusively stable in $1+$ charge state ($H_i^+$), acting as a shallow donor. Our calculated result for $H_i$ is in good agreement with recent calculations based on the HSE06-screened hybrid-functional [41]. The shallow donor behavior of $H_i$ was also reported in other oxide semiconductors. In addition, the migration barrier for $H_i$ was reported to be as low as 0.25 eV, indicating that it is highly mobile even at a very low temperature, unless it is trapped by other defects [42]. Indeed, $H_i^+$ can be trapped by $N_O$ acceptors through Coulombic attraction. Figure 4(a) shows the calculated formation energies of the $N_O$-$H_i$ complex, $H_i$, and $N_O$ in $SrTiO_3$ under O-poor conditions. $N_O$-$H_i$ is stable in $1+$ and neutral charge states with the transition level $(+/0)$ located at 1.23 eV above the VBM. This behavior of $N_O$-$H_i$ in $SrTiO_3$ is not the same as in $TiO_2$ where $N_O$-$H_i$ is only stable in the neutral charge state [28]. In $TiO_2$, H completely passivates the localized state of $N_O^-$ that appears in the band gap. In $SrTiO_3$, H partially passivates one of the localized states of $N_O^-$, leaving another N-related state in the band gap. Figure 5 illustrates the schematic diagram of the $N_O$ $2p$ and $H_i$ $s$ hybridization in $TiO_2$ and $SrTiO_3$. In $TiO_2$, two electrons from $N_O^-$ $2p$ occupy the bonding state and lay deep in the valence band, leaving the empty antibonding state resonant in the conduction band [Fig. 5(a)]. Therefore, the localized gap state is absent and $N_O$-$H_i$ exists only in the neutral charge state. In $SrTiO_3$, $N_O^-$ induces two nearly degenerate states, fully occupied by four electrons. This difference is a result of the difference in coordination number of N in $TiO_2$ and $SrTiO_3$; in $TiO_2$, N is threefold coordinated, while in $SrTiO_3$, N is twofold coordinated. Thus, two nonbonding states are present in the band gap in the case of $SrTiO_3$, while only one nonbonding state is present in the case of $TiO_2$. While one of the two occupied states participates in the $N_O$ $2p$ and $H_i s$ hybridization in $SrTiO_3$, another state does

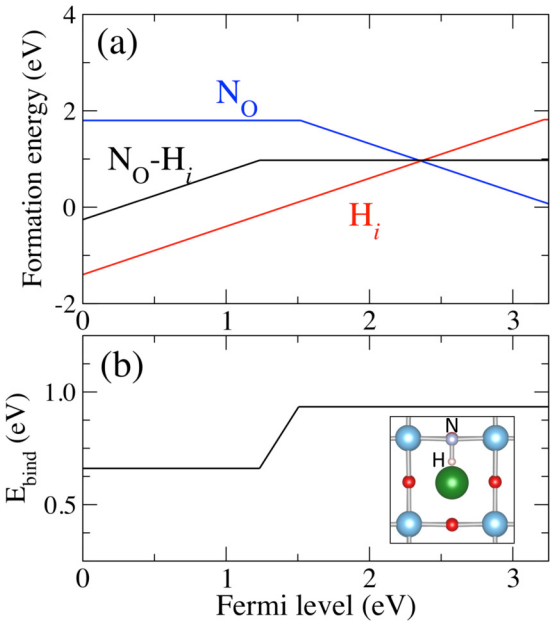


FIG. 4. (a) Formation energies of $N_O$, $H_i$, and the $N_O$-$H_i$ complex under the O-poor condition, and (b) the calculated binding energy of $N_O$-$H_i$ as a function of the Fermi level (see more details in the text). Inset shows the local atomic structure of $N_O$-$H_i$.

not and resides in the band gap [Fig. 5(b)]. An electron can be removed from this state, resulting in $(N_O\text{-}H_i)^+$. We also considered the optical transition associated with the process $(N_O\text{-}H_i)^0 + h\nu \rightarrow (N_O\text{-}H_i)^+ + e^-$, in which an electron is excited from $(N_O\text{-}H_i)^0$ to the conduction band. The calculated absorption energy is 2.76 eV, which is higher than the absorption energy associated with $N_O$. This absorption energy is in good agreement with the experimental observations in N-doped $SrTiO_3$ samples which was synthesized under high hydrogen content [16] or $NH_3$ as nitridizing source [43]. The optical absorption edges of these samples were reported to be about 2.64–2.75 eV.

We also calculated the binding energy of the $N_O$-$H_i$ complex, defined as

$$E_b[(N_O\text{-}H_i)^q] = E^f\left[N_O^{q'}\right] + E^f[H_i^+] - E^f[(N_O\text{-}H_i)^q], \quad (2)$$

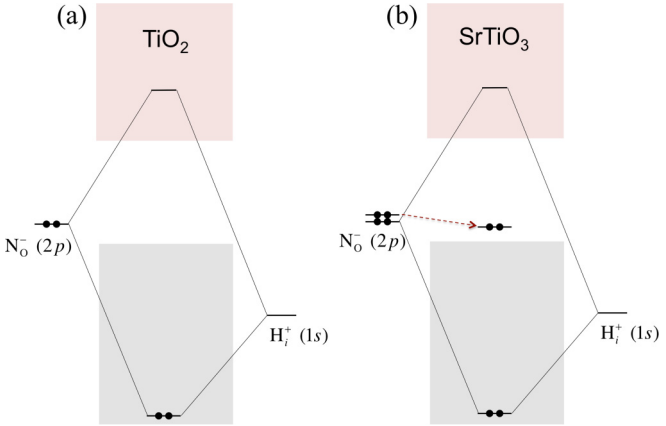


FIG. 5. Schematic diagram for the $N_O$ and $H_i$ hybridization of the $N_O$-$H_i$ complex in (a) $TiO_2$ and (b) $SrTiO_3$.

where $E^f[(N_O\text{-}H_i)^q]$ is the formation energy of the complex in charge state $q(q = 0,+)$, and $E^f[N_O^{q'}]$ is the formation energy of $N_O$ in charge state $q'$ $(q' = 0, -)$. The calculated binding energy is shown as a function of Fermi level in Fig. 4(b). The binding energy for $(N_O\text{-}H_i)^0$ is 0.94 eV, which is higher than that in the case of $TiO_2$ (0.58 eV in rutile and 0.49 eV in anatase) [28]. However, the binding energy is reduced to 0.66 eV for $(N_O\text{-}H_i)^+$ when the Fermi level moved toward the valence band. Note that the binding energies are unchanged for higher O chemical potentials. To address the stability of the complex, we estimated its dissociation energy, given by $E_b[(N_O\text{-}H_i)^0] + E_m(H_i^+)$, to be 1.2 eV, where $E_m(H_i^+)$ is the calculated migration barrier of interstitial hydrogen of 0.25 eV [42]. Thus, $(N_O\text{-}H_i)^0$ is expected to be stable at temperatures up to ~465 K. Our results indicated that the presence of H does not completely reverse the visible-light absorption capability of N-doped $SrTiO_3$, instead it causes a blueshift of the absorption edge.

### F. Vibrational frequencies of N impurities

To facilitate experimental identification through vibrational spectroscopy, we also calculated the local vibrational modes (LVM) associated with $(NO)_O$, $(NO_2)_{2O}$, $(N_2)_O$, $(N_2)_{2O}$, and $N_O$-$H_i$. The stretching vibrational modes of the N-related molecules were calculated using the approach described in Ref. [44], except for $(NO_2)_{2O}$. The vibrational mode frequencies of $(NO_2)_{2O}$ were calculated by solving the dynamical matrix associated with small displacements of N and the two nearest O atoms as described in Ref. [45]. For $(NO)_O$, $(N_2)_O$, and $(N_2)_{2O}$, we slightly and equally displaced either N–N or N–O atoms to calculate the potential energy of stretching and compressing bonds because they have similar masses. For $N_O$-$H_i$, only H was displaced because it has a much smaller mass compared to N or O. The vibration frequency, including the anharmonic contribution, can then be calculated from the coefficients of a fourth-degree polynomial [44]. Note that the anharmonic contribution to $(NO_2)_{2O}$ is estimated to be equal to that of the NO molecule. Our calculated stretching vibrational modes of the free molecules are in reasonably good agreement with the experimental measurements, i.e., 2532 $cm^{-1}$ (cal.) versus 2358 $cm^{-1}$ for $N_2$,2115 $cm^{-1}$ (cal.) versus 1904 $cm^{-1}$ for NO, 3404 $cm^{-1}$ (cal.) versus 3337 $cm^{-1}$ for $NH_3$ (symmetric mode), and 1439 $cm^{-1}$ (cal.) versus 1318 $cm^{-1}$ for $NO_2$ (symmetric mode). Notably, the calculated values are 7.4%, 11.1%, 2.0%, and 9.2% larger than the measured values for $N_2$, NO, $NH_3$, and $NO_2$, respectively. To reduce these systematic errors, we scaled down the calculated vibrational frequencies ($\omega_{calculated}$ in Table I) for $(NO)_O$ by 11.1%, $(N_2)_O$ and $(N_2)_{2O}$ by 7.4%, $N_O$-$H_i$ by 2.0%, and $(NO_2)_{2O}$ by 9.2% ($\omega_{corrected}$). Table I shows that the calculated stretching LVM frequencies associated with $(NO)_O$, $(N_2)_O$, $(N_2)_{2O}$, and $(NO_2)_{2O}$ vary between ~600 and 2400 $cm^{-1}$. As the charge state changed by adding electrons to the defect state, the LVM frequencies associated with $(NO)_O$, $(N_2)_O$, $(N_2)_{2O}$, and $(NO_2)_{2O}$ decreased as a result of adding electrons into the antibonding $pp\pi^*$ molecular orbitals, which led to an increase in the bond lengths and weaker N–N and N–O bonds. In contrast, the LVM frequency of $(N_O\text{-}H_i)^+$ is lower than that of $(N_O\text{-}H_i)^0$ as a result of a weaker N-H bond due to the

TABLE I. Calculated bond lengths and stretching LVM frequencies of selected free molecules and N defects. The experimental stretching LVM frequencies of the free molecules and $H_i$ are listed in the last column.

| Free molecules/defects | Bond type | Charge state ($q$) | $d$ (Å) | $\omega_{\text{calculated}}(\text{cm}^{-1})$ | $\omega_{\text{exp}}/\omega_{\text{corrected}}(\text{cm}^{-1})$ |
|---|---|---|---|---|---|
| NO | N–O | | 1.155 | 2115 | 1904 |
| $NO_2$ | N–O | | 1.193 | 1439 | 1318 |
| $N_2$ | N–N | | 1.106 | 2532 | 2359 |
| $NH_3$ | N–H | | 1.016 | 3404 | 3337 |
| $(NO)_O$ | N–O | + | 1.250 | 1574 | 1400 |
| | | 0 | 1.310 | 1340 | 1191 |
| | | − | 1.415 | 1104 | 982 |
| $(NO_2)_{2O}$ | N–O | 3+ | 1.254 | 1371 | 1261 |
| | | 2+ | 1.351 | 812 | 737 |
| | | + | 1.479 | 626 | 568 |
| $(N_2)_O$ | N–N | 2+ | 1.118 | 2363 | 2188 |
| | | + | 1.162 | 2071 | 1918 |
| | | 0 | 1.235 | 1856 | 1719 |
| | | − | 1.284 | 1443 | 1337 |
| $(N_2)_{2O}$ | N–N | 4+ | 1.123 | 2299 | 2129 |
| | | 3+ | 1.172 | 1993 | 1846 |
| | | 2+ | 1.224 | 1679 | 1555 |
| | | + | 1.322 | 1240 | 1149 |
| | | 0 | 1.428 | 913 | 845 |
| $N_O$-$H_i$ | N–H | + | 1.021 | 3359 | 3291 |
| | | 0 | 1.015 | 3418 | 3349 |
| $H_i$ | | + | 0.967 | 3408 | 3500 |

weaker Coulombic attraction between $N_O^0$ and $H_i^+$. As shown in Table I, it is feasible to distinguish between $N_O$-$H_i$ and other N defects as their LVM frequencies differ by $\sim$1100 $\text{cm}^{-1}$. For comparison, we calculated the LVM of the O–H bond associated with $H_i^+$ as $\sim$3408 $\text{cm}^{-1}$, which is in reasonable agreement with the previous calculation and measured value of $\sim$3500 $\text{cm}^{-1}$ [41].

## IV. CONCLUSION

In summary, we have investigated the thermodynamic stability and the effects of N impurities on the optical absorption in $SrTiO_3$ using hybrid density-functional calculations. We find that substitutional $N_O$ is a deep acceptor that is energetically favorable over other N impurity configurations in $n$-type $SrTiO_3$. Our calculations show that $N_O$ gives rise to optical absorption in the visible region, which is consistent with the experimental observations. We also find that hydrogen can bind with $N_O$. In contrast to $TiO_2$, the formation of the $N_O$-$H_i$ complex in $SrTiO_3$ does not completely reverse the $N_O$-induced visible-light absorption, yet it leads to a blueshift in the absorption edge. Our results indicate that $N_O$-$H_i$ can explain the observed optical absorption in samples prepared with highly H-contained nitridizing sources. The higher binding energy of $N_O$-$H_i$ in $SrTiO_3$ compared to that in $TiO_2$ indicates that higher-temperature thermal annealing is needed to remove H and restore the optical properties of $N_O$. Our results suggest that other N configurations also contribute to optical absorption in the visible range. In addition, we find that $(N_2)_{2O}$ acts as an active compensating donor for the $N_O$ acceptor. Therefore, N is unlikely to be a good $p$-type dopant for $SrTiO_3$. Our calculated LVM frequencies for N impurities including the $N_O$-$H_i$ complex will serve as a guide for examining various N configurations and the effect of H in N-doped $SrTiO_3$ experimentally.

## ACKNOWLEDGMENTS

This work is supported by The Thailand Research Fund (Contract No. TRG 5780260) and Institute for Promotion of Science and Technology (DPST Research Grant 036/2557). P.R. and J.T-T. acknowledge Kasetsart University Research and Development Institute (KURDI). We wish to thank the High-Performance Computing Center at Synchrotron Light Research Institute (SLRI, Thailand) for their hospitality.

[1] A. Fujishima and K. Honda, Nature (London) **238**, 37 (1972).
[2] H. Tong, S. Ouyang, Y. Bi, N. Umezawa, M. Oshikiri, and J. Ye, Adv. Mater. **24**, 229 (2012).
[3] Y. Xu and M. A. A. Schoonen, Am. Mineral. **85**, 543 (2000).
[4] R. Konta, T. Ishii, H. Kato, and A. Kudo, J. Phys. Chem. B **108**, 8992 (2004).
[5] H. Kato and A. Kudo, J. Phys. Chem. B **106**, 5029 (2002).
[6] T. Ishii, H. Kato, and A. Kudo, J. Photochem. Photobiol., A **163**, 181 (2004).

[7] D. Wang, J. Ye, T. Kako, and T. Kimura, J. Phys. Chem. B **110**, 15824 (2006).
[8] P. Reunchan, S. Ouyang, N. Umezawa, H. Xu, Y. Zhang, and J. Ye, J. Mater. Chem. A **1**, 4221 (2013).
[9] Y. Y. Mi, S. J. Wang, J. W. Chai, J. S. Pan, C. H. A. Huan, Y. P. Feng, and C. K. Ong, Appl. Phys. Lett. **89**, 231922 (2006).
[10] S. Yoon, A. E. Maegli, L. Karvonen, S. K. Matam, A. Shkabko, S. Riegg, T. Großmann, S. G. Ebbinghaus, S. Pokrant, and A. Weidenkaff, J. Solid State Chem. **206**, 226 (2013).
[11] J. Wang, S. Yin, M. Komatsu, and T. Sato, J. Eur. Ceram. Soc. **25**, 3207 (2005).
[12] J. Wang, S. Yin, M. Komatsu, Q. Zhang, F. Saito, and T. Sato, Applied Catal., B **52**, 11 (2004).
[13] J.-H. Yan, Y.-R. Zhu, Y.-G. Tang, and S.-Q. Zheng, J. Alloys Compd. **472**, 429 (2009).
[14] J. Wang, H. Li, H. Li, S. Yin, and T. Sato, Solid State Sci. **11**, 182 (2009).
[15] M. Miyauchi, M. Takashio, and H. Tobimatsu, Langmuir **20**, 232 (2003).
[16] J. Wang, S. Yin, M. Komatsu, Q. Zhang, F. Saito, and T. Sato, J. Photochem. Photobiol., A **165**, 149 (2004).
[17] T. Sun and M. Lu, Appl. Surf. Sci. **274**, 176 (2013).
[18] R. Asahi, T. Morikawa, T. Ohwaki, K. Aoki, and Y. Taga, Science **293**, 269 (2001).
[19] C. Zhang, Y. Jia, Y. Jing, Y. Yao, J. Ma, and J. Sun, Comput. Mater. Sci. **79**, 69 (2013).
[20] W. Wei, Y. Dai, M. Guo, L. Yu, and B. Huang, J. Phys. Chem. C **113**, 15046 (2009).
[21] B. Modak, K. Srinivasu, and S. K. Ghosh, Phys. Chem. Chem. Phys. **16**, 24527 (2014).
[22] B. Modak, K. Srinivasu, and S. K. Ghosh, RSC Adv. **4**, 45703 (2014).
[23] B. Modak and S. K. Ghosh, J. Phys. Chem. C **119**, 23503 (2015).
[24] W. Wei, Y. Dai, M. Guo, L. Yu, H. Jin, S. Han, and B. Huang, Phys. Chem. Chem. Phys. **12**, 7612 (2010).
[25] H. Liu, H. Dong, X. Meng, and F. Wu, Chem. Phys. Lett. **555**, 141 (2013).
[26] P. Liu, J. Nisar, B. Pathak, and R. Ahuja, Int. J. Hydrogen Energy **37**, 11611 (2012).
[27] C. M. Liu, X. T. Zu, and W. L. Zhou, J. Phys. D: Appl. Phys. **40**, 7318 (2007).
[28] J. B. Varley, A. Janotti, and C. G. Van de Walle, Adv. Mater. **23**, 2343 (2011).
[29] P. Reunchan, N. Umezawa, S. Ouyang, and J. Ye, Phys. Chem. Chem. Phys. **14**, 1876 (2012).
[30] J. Heyd, G. Scuseria, and M. Ernzerhof, J. Chem. Phys. **118**, 8207 (2003).
[31] G. Kresse and J. Furthmüller, Comput. Mater. Sci. **6**, 15 (1996).
[32] P. E. Blöchl, Phys. Rev. B **50**, 17953 (1994).
[33] K. Van Benthem, C. Elsässer, and R. H. French, J. Appl. Phys. **90**, 6156 (2001).
[34] A. Okazaki and M. Kawaminami, Mater. Res. Bull. **8**, 545 (1973).
[35] A. Janotti, J. B. Varley, M. Choi, and C. G. Van de Walle, Phys. Rev. B **90**, 085202 (2014).
[36] C. Freysoldt, B. Grabowski, T. Hickel, J. Neugebauer, G. Kresse, A. Janotti, and C. G. Van de Walle, Rev. Mod. Phys. **86**, 253 (2014).
[37] C. Freysoldt, J. Neugebauer, and C. G. Van de Walle, Phys. Status Solidi B **248**, 1067 (2011).
[38] J. L. Lyons, A. Janotti, and C. G. Van de Walle, Appl. Phys. Lett. **95**, 252105 (2009).
[39] See Supplemental Material at http://link.aps.org/supplemental/10.1103/PhysRevB.95.205204 for the formation energy of N-related defects under a high N-doping condition.
[40] W.-J. Yin, S.-H. Wei, M. M. Al-Jassim, and Y. Yan, Phys. Rev. Lett. **106**, 066801 (2011).
[41] J. B. Varley, A. Janotti, and C. G. Van de Walle, Phys. Rev. B **89**, 075202 (2014).
[42] J. T-Thienprasert, I. Fongkaew, D. J. Singh, M.-H. Du, and S. Limpijumnong, Phys. Rev. B **85**, 125205 (2012).
[43] I. Marozau, A. Shkabko, G. Dinescu, M. Döbeli, T. Lippert, D. Logvinovich, M. Mallepell, C. W. Schneider, A. Weidenkaff, and A. Wokaun, Appl. Surf. Sci. **255**, 5252 (2009).
[44] S. Limpijumnong, J. E. Northrup, and C. G. Van de Walle, Phys. Rev. B **68**, 075206 (2003).
[45] J. T-Thienprasert, S. Limpijumnong, A. Janotti, C. G. Van de Walle, L. Zhang, M. H. Du, and D. J. Singh, Comput. Mater. Sci. **49**, S242 (2010).